NANO LETTERS

Letter

pubs.acs.org/NanoLett

Vapor-Condensation-Assisted Optical Microscopy for Ultralong Carbon Nanotubes and Other Nanostructures

Jiangtao Wang, Tianyi Li, Bingyu Xia, Xiang Jin, Haoming Wei, Wenyun Wu, Yang Wei,* Jiaping Wang, Peng Liu, Lina Zhang, Qunqing Li, Shoushan Fan, and Kaili Jiang*

State Key Laboratory of Low-Dimensional Quantum Physics, Department of Physics and Tsinghua-Foxconn Nanotechnology Research Center, Tsinghua University, Beijing 100084, China

Supporting Information

ABSTRACT: Here we present a simple yet powerful approach for the imaging of nanostructures under an optical microscope with the help of vapor condensation on their surfaces. Supersaturated water vapor will first form a nanometer-sized water droplet on the condensation nuclei on the surface of nanostructures, and then the water droplet will grow bigger and scatter more light to make the outline of the nanostructure be visible under dark-field optical microscope. This vapor-condensation-assisted (VCA) optical microscopy is applicable to a variety of nanostructures from ultralong carbon nanotubes to functional groups, generating images with contrast coming from the difference in density of the condensation sites, and does not induce any impurities to the specimens. Moreover, this low-cost and efficient technique can be conveniently integrated with other facilities, such as Raman spectroscope and so forth, which will pave the way for widespread applications.

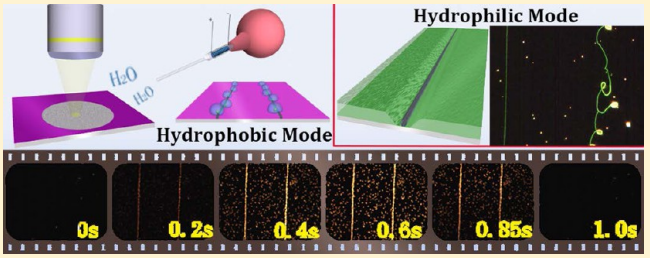

KEYWORDS: *Vapor condensation, optical microscopy, carbon nanotube, imaging*

Seeing is believing. An accurate and efficient imaging of nanostructures can significantly deepen our understanding of the microscopic world and shed light on prospective applications. Compared with scanning electron microscope (SEM),[1] transmission electron microscope (TEM),[2] atomic force microscope (AFM),[3] scanning tunneling microscope (STM),[4] and so forth, it is very easy to operate an optical microscope and quite convenient to integrate it with other facilities. However, nanomaterials or nanostructures such as carbon nanotubes (CNTs) cannot be directly observed by optical microscope, because their nanoscale dimensions are much smaller than the wavelength of visible light. Therefore, the visualization of nanomaterials, especially of CNTs by optical microscopy, is highly desirable and has long been attempted.

In 2009, Chang and colleagues reported a method to make CNTs optically observable by coating them with carbon shells 100−1500 nm in thickness by chemical vapor deposition (CVD).[5] To some extent, this method was helpful to study the growth of CNTs. However, further measurements and applications of these CNTs were heavily restricted because the outer carbon shells would weaken the outstanding mechanical and electrical properties of CNTs. Another approach of depositing Ag, Au, or TiO_2 nanoparticles onto CNTs was developed recently.[6−8] With this technique, CNTs either on a substrate or suspended in air can be visualized under an optical microscope. However, the deposition process, either in liquid phase or in vapor phase, was relatively complicated. Moreover, it was difficult to remove the nanoparticles on CNTs, thus again hindering further measurements and applications. Therefore, visualizing nanomaterials nondestructively and efficiently under an optical microscope remains a significant challenge.

Vapor condensation is a ubiquitous phenomenon in our daily life. From the formation of dewdrop to the water cycle in meteorology, vapor condensation has been intensively studied as a natural phenomenon. Even in elementary particle physics, vapor condensation has long been used in the Wilson cloud chamber to detect high energy particles.[9,10] When a high energy charged particle enters the chamber, it will ionize the supersaturated vapor of water or alcohol. With the resulting ions as condensation nuclei, visible mist will form along the track of the particle. Here we show that such principle can also be applied to visualizing nanomaterials or nanostructures. As warm water vapor is blown onto the sample, it will condense on some nuclei attached to the sample. Meanwhile, the outlines of the nanostructures can be clearly observed under an optical microscope. In a few seconds, the condensed water will evaporate spontaneously, leaving samples clean as before. This vapor-condensation-assisted (VCA) optical microscopy is extremely powerful in characterizing ultralong CNTs and can also be used to observe other nanostructures, even functional

Received: March 27, 2014
Published: May 22, 2014

   dx.doi.org/10.1021/nl5016969 | *Nano Lett.* 2014, 14, 3527−3533

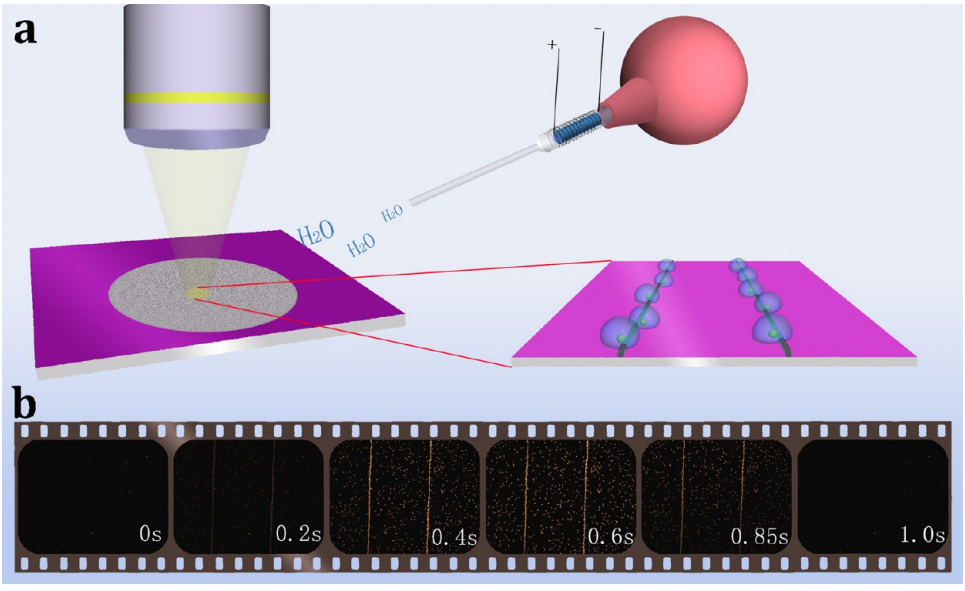

Figure 1. Vapor-condensation-assisted (VCA) visualization of ultralong CNTs. (a) A schematic diagram of the experimental setup. Warm water vapor is blown from a homemade apparatus and condensed onto the sample. As water microdroplets form along the CNTs, the outlines of CNTs can be observed under a dark-field optical microscope. (b) Screenshots of a streaming video, illustrating the whole process of VCA visualization of ultralong CNTs under an optical microscope.

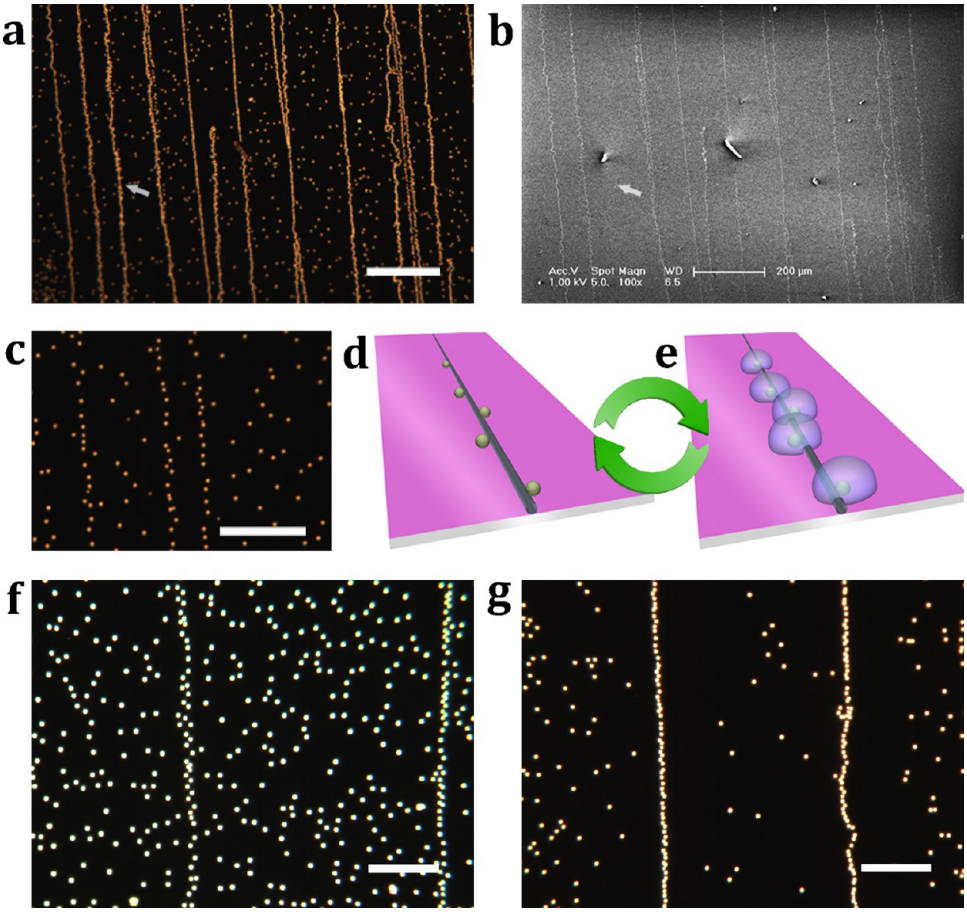

Figure 2. VCA imaging of ultralong CNTs on silicon substrates. (a) The VCA image and (b) the corresponding SEM image of ultralong CNTs on a silicon substrate with a thermal oxide layer. The white arrows indicate a CNT visible in the VCA image but invisible by SEM. Scale bars: 200 μm. (c) A higher-magnification VCA image of CNTs showing that the outlines of CNTs are composed of a series of bright dots. Scale bar: 100 μm. (d,e) Schematic diagrams showing that warm water vapor condenses on some nuclei attached to the CNTs, forming microdroplets visible under optical microscope. (f) The VCA image of ultralong CNTs on silicon substrate with a 1 μm silicon nitride layer. Scale bar: 50 μm. (g) The VCA image of ultralong CNTs on silicon substrate with a naturally oxidized layer. Scale bar: 50 μm.

dx.doi.org/10.1021/nl5016969 | *Nano Lett.* 2014, 14, 3527−3533

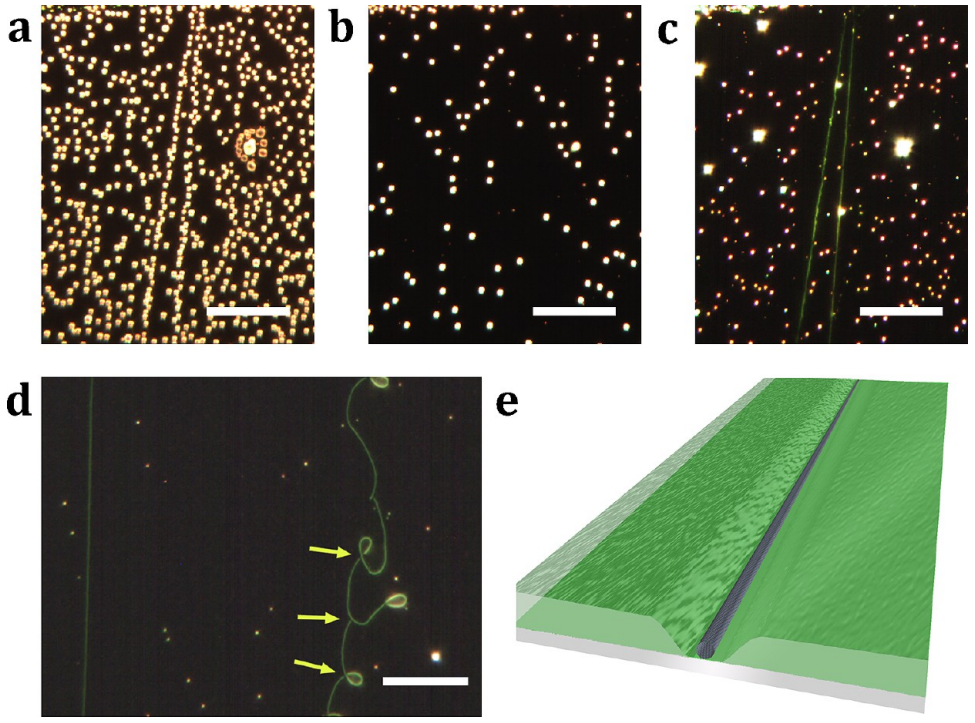

Figure 3. VCA imaging of clean ultralong CNTs on silicon substrate. (a) The VCA image of as-grown ultralong CNTs. (b) The VCA image of clean ultralong CNTs after annealing in hydrogen showing no contrast. (c) The VCA image showing that clean ultralong CNTs can be observed as continuous lines after the substrate is transformed to more hydrophilic. (d) The VCA image of intersecting ultralong CNTs. The yellow arrow indicates that there is a disconnection at the crossing. Scale bars: 50 μm. (e) The schematic diagram of the visualization of clean CNTs on hydrophilic substrate. The hydrophobic CNTs act as boundaries of water films.

groups, leading to widespread applications in the immediate future.

Figure 1a schematically shows the experimental setup of the VCA optical visualization technique, which includes a dark-field optical microscope and a homemade water vapor blower (details can be found in Methods). Because of their diameters of a few nanometers, ultralong CNTs cannot be directly observed under an optical microscope. However, as we blow some warm water vapor to the sample, all of the CNTs on the substrate can be seen clearly under an optical microscope (Figure 1b). The image of CNTs would disappear spontaneously in a few seconds after we stop blowing. Fortunately, this simple imaging strategy can be repeated many times and a few seconds actually is long enough to take a clear image of the CNTs. The video of the whole process can be seen in Supporting Information.

Figure 2a,b compares the VCA image and the SEM image of as-grown ultralong CNTs on the same area of a silicon substrate with a thermal oxide layer of 500 nm. It is evident that the VCA image exactly shows the location and the morphology of the ultralong CNTs (see Supporting Information). In fact, there is a CNT visible in the VCA image (indicated by the white arrow in Figure 2a), but invisible in the low-voltage SEM image (where the white arrow locates in Figure 2b). This may be due to the special contrast mechanism of low-voltage SEM.[11,12] By switching to a higher-magnification objective, we can clearly see that the outlines of CNTs are not continuous but are composed of a series of bright dots (Figure 2c), indicating that what we see on the VCA image are not "real" CNTs but the outlines of CNTs.

Considering that the bright dots will disappear spontaneously, we deduce that the outlines of CNTs are made up of water droplets attached to CNTs. Thus, a reasonable imaging mechanism is as follows. When reaching the sample, the warm water vapor would condense into microdroplets on the condensation nuclei attached to the samples. Under oblique illuminating light, the microdroplets of water will act as scattering centers, appearing as bright dots under a dark-field optical microscope. Particularly, due to the high physical or chemical activity of some impurities (e.g., amorphous carbon or some functional groups) attached to CNTs, the condensation nuclei appear denser along the CNTs than on other parts of the substrate, sketching the outlines of CNTs (Figure 2d,e). Once the blowing stops, the water droplets begin to evaporate, thus the outlines of CNTs disappear. Thanks to this mechanism, the reversible and repeatable imaging of CNTs can be easily understood. Furthermore, by repeating the imaging process, we found that the number and the position of the bright dots along CNTs seldom change, which is strong evidence that the imaging process does not induce new impurities to the CNTs.

Further experiments revealed that VCA imaging also works well with other kinds of substrates. Figure 2f,g shows the VCA images of ultralong CNTs on a silicon substrate with a 1 μm silicon nitride layer and on a silicon substrate with a naturally oxidized layer, respectively. In both cases, the position and morphology of ultralong CNTs can be clearly discerned from the VCA images.

The aforementioned imaging mechanism relies on the impurities on CNTs as condensation nuclei, which should be amorphous carbon or other functional groups that are attached to CNTs during the growth process. We demonstrate here that the VCA visualization still works well with clean CNTs without impurities. Figure 3a shows the VCA image of as-grown ultralong CNTs on a silicon substrate with a thermal oxide

dx.doi.org/10.1021/nl5016969 | *Nano Lett.* 2014, 14, 3527−3533

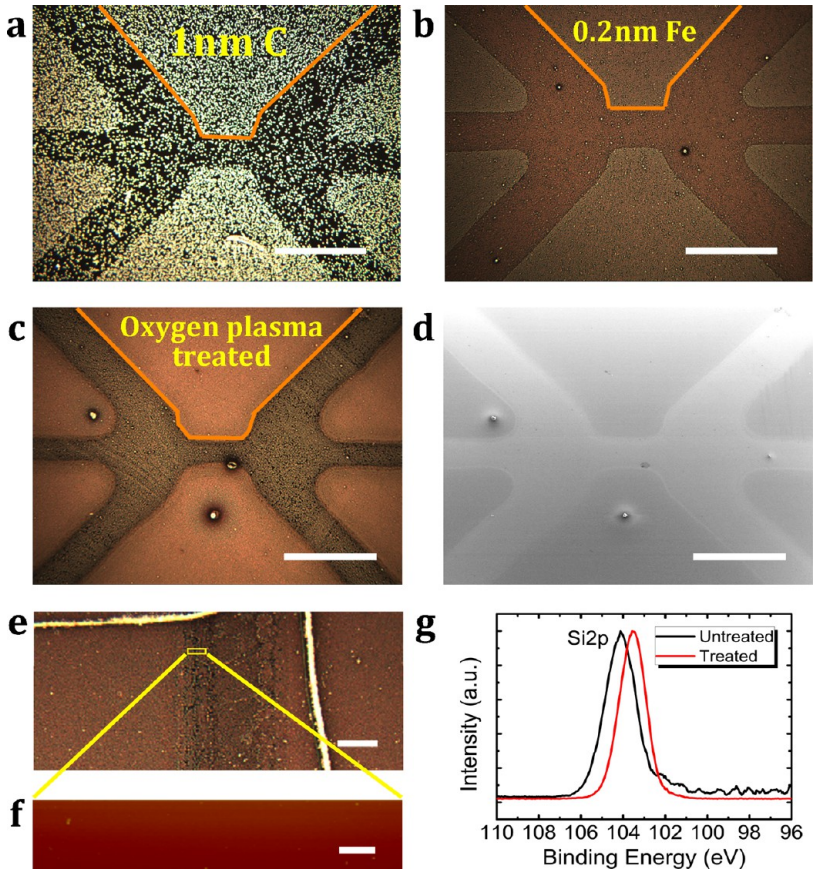

Figure 4. Characterization of nanostructures on silicon substrates. (a) The VCA image of the deposited pattern of 1 nm amorphous carbon. (b) The VCA image of the deposited pattern of 0.2 nm Fe. (c) The VCA image and (d) the corresponding SEM image of the pattern selectively treated by oxygen plasma. Scale bars: 500 μm. The VCA image shows a better contrast than the SEM image. (e) A higher-magnification VCA image of the boundary between the treated and the untreated areas. Scale bar: 100 μm. (f) The AFM image of selected area in (e) shows no contrast. Scale bar: 4 μm. (g) A comparison of the XPS of the treated and untreated silicon substrates.

layer. By annealing as-grown samples in a hydrogen atmosphere at 700 °C, amorphous carbon can be removed from CNTs, therefore the VCA image cannot show the outlines of clean CNTs (Figure 3b). However, after treated by argon plasma for 10 s, the CNTs on the substrate appear as continuous bright lines in the VCA image (Figure 3c and Supporting Information). Note that wherever the CNT in this image makes a crossing with itself, there appears a disconnection (Figure 3d). Furthermore, by carefully investigating the process that the CNTs emerge in slow motion, we found that small water droplets were formed on the substrate at first. And then small droplets gradually merge into bigger ones as their size grows. Finally, all the droplets merge into water films separated by the CNTs.

On the basis of the facts above, we deduce that the substrates have turned hydrophilic after treated by argon plasma. To verify this point, we measured the contact angle between water and the substrate. Before being treated by argon plasma, the contact angle on the silicon substrate was 84°, in which water droplets tended not to merge into bigger ones. After being treated by argon plasma, the contact angle was as small as 11°, thus the water droplets tended to merge with each other and finally form water films. However, CNTs themselves are hydrophobic and strongly attached to the substrate. Therefore, CNTs can act as boundaries between these water films and prevent them from further merging, appearing as continuous lines (Figure 3e). As a result, what we see using an optical microscope is again the outlines of CNTs but not CNTs themselves. This illustration is strongly confirmed by the disconnection at the crossing. At the crossing, there has to be a segment of CNT that is not attached closely to the substrate. Therefore, the water films on both sides can merge beneath this segment of CNT, making this segment of CNT unobservable. Besides, we also tested other kinds of hydrophilic substrates including silicon substrates with a thermal oxide layer further deposited with Al or Ti, and the CNTs similarly appear as continuous bright lines. The visualization of CNTs on hydrophilic substrates is of great importance, because it does not rely on impurities on CNTs and extends the VCA imaging technique to very clean CNTs.

Here we'd like to stress that the contrast of VCA images of CNTs comes from the difference in density of condensation sites. For as-grown ultralong CNTs, the density of condensation sites on the CNT's surface is larger than that on the hydrophobic substrate, resulting in a distinct outline of CNT in VCA image. However, for clean CNT after removing the condensation sites, a hydrophilic substrate with tremendous condensation sites will generate a very thin water film but separated by the hydrophobic CNTs, again creating a distinct outline of CNT in VCA image. In the case of the as-grown CNTs with condensation sites, the resolution of VCA imaging is limited by the density of the condensation sites, which is around tens of micrometers depending on the growth conditions. But for clean CNTs after removing condensation

dx.doi.org/10.1021/nl5016969 | *Nano Lett.* 2014, 14, 3527−3533

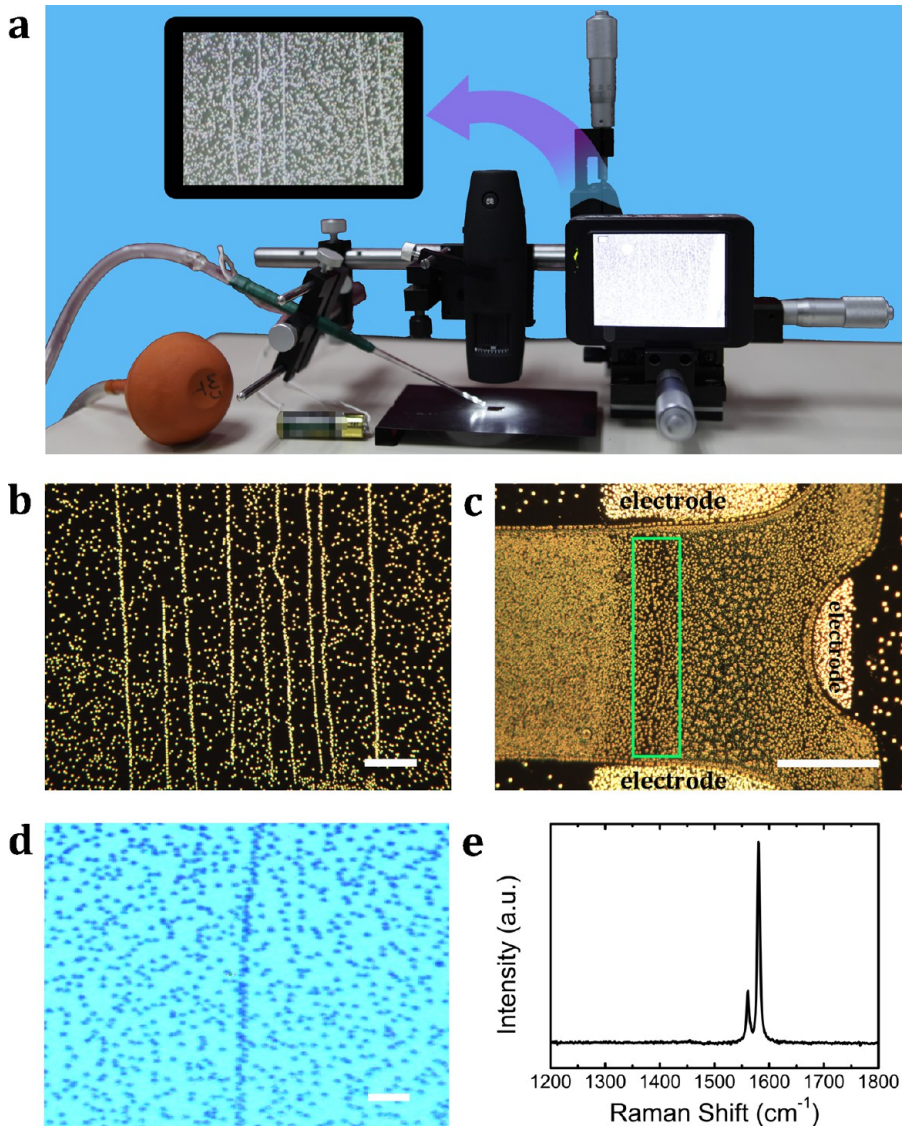

Figure 5. Applications of VCA optical microscopy. (a) A simple and very low-cost VCA optical microscope system. VCA images of ultralong CNTs (inset) can be easily obtained by this simple system. (b) The VCA image of ultralong CNTs on the intrinsic silicon substrate with very high resistivity. (c) The VCA image of a device with an ultralong CNT located in the green box. Scale bars: 100 μm. (d) The VCA image of an ultralong CNT acquired by a Raman system. Scale bar: 10 μm. (e) The Raman spectrum of the CNT in (d).

sites, the resolution is determined by the diffraction limit of the optical microscope.

To step forward, we find that the VCA technique is not limited to observing CNTs but is also able to characterize other nanostructures on substrates. Figure 4a,b shows the VCA images of a thin layer of deposited amorphous carbon and Fe, respectively. Note that the deposited layer with a thickness of no more than 1 nm can hardly be observed by conventional optical microscopes either in the bright-field mode or in the dark-field mode. However, once water vapor is blown to the substrate, the areas with and without deposited layers show a strong contrast due to the divergence in the density of condensation nuclei.

It is more interesting that the VCA technique is very sensitive to surface functional groups on the substrate. It has been reported that oxygen plasma treatment can change the surface functional groups on a silicon substrate with a thermal oxide layer.[13−15] The pattern of the area treated by oxygen plasma can be easily observed by the VCA optical microscope (Figure 4c) and by SEM (Figure 4d). There is no doubt that the optical image shows much better contrast than the SEM image and provides more detailed information. Those functional groups even cannot be imaged by AFM, as Figure 4e,f shows, probably because they do not form a dense layer on the substrate. However, a comparison of X-ray photoelectron spectra (XPS) of the treated and the untreated substrates (Figure 4g) shows that there is truly some changes in surface functional groups on the silicon substrate. The VCA imaging technique is indeed very sensitive to this change in surface functional groups and provides good contrast for it.

Although the VCA imaging technique is of lower resolution than electron microscopy, it is rather competitive in certain cases owing to its simplicity, efficiency, and low cost. Actually, we have built a simple and very low-cost VCA optical microscope system in our laboratory (Figure 5a), which consists of a hand-held microscope and a homemade water vapor blower. VCA images of ultralong CNTs can be easily obtained by this simple system.

dx.doi.org/10.1021/nl5016969 | Nano Lett. 2014, 14, 3527−3533

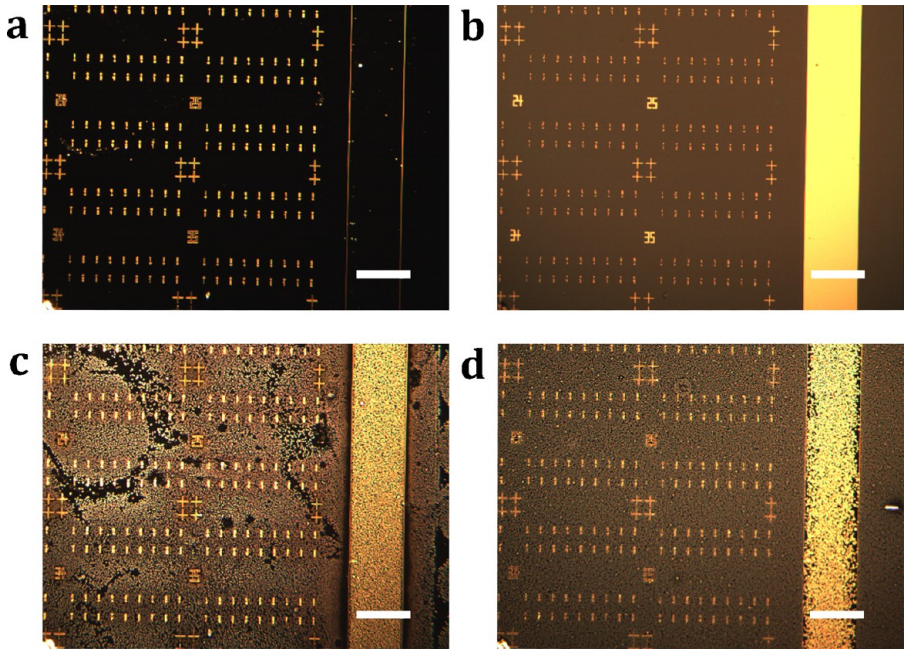

Figure 6. Application of VCA optical microscopy to image residual photoresist. Neither (a) the dark-field nor (b) the bright-field optical image can prove the existence of the residual photoresist. (c) The VCA image clearly showing the residual photoresist with dark contrast. (d) The VCA image after the removal of the residual photoresist. Scale bars: 200 μm.

With regards to ultralong CNTs, the VCA imaging can offer an immediate feedback of the density and the morphology of the CNTs, thus allowing researchers to optimize the growth condition more efficiently. Furthermore, this technique can be applied to certain cases where traditional characterization methods are not applicable. For instance, if CNTs are grown on a substrate with high resistivity such as intrinsic silicon substrates, we can hardly obtain a clear image of CNTs through SEM. However, due to the novel mechanism of the VCA visualization method, we can still clearly observe them by an optical microscope (Figure 5b).

The easy accessibility of optical microscopes allows the VCA optical microscopy to be easily integrated with other experiments. Figure 5c shows the VCA image of an ultralong CNT with an electrode on each end. Thanks to the large field of view of optical microscope, we can easily obtain the relative location of the CNT and the electrodes, which can be very helpful for fabricating nanodevices based on ultralong CNTs. Another good example is to integrate the VCA characterization method with Raman spectroscopy. Generally, if we want to acquire the Raman spectra of CNT samples with a relatively low density, we need to do large-area mapping to locate the CNTs, which is rather time-consuming. However, by applying the VCA method, we can directly "see" the locations of CNTs using the optical microscope of Raman spectroscope, and the mapping process is considerably simplified (Figure 5d,e).

Finally, we would like to show that the VCA optical microscopy can have important applications in semiconductor industry. As is well-known, photoresist is among the most frequently used material in semiconductor industries. A trace amount of residual photoresist after photolithography will severely affect the performance of as-fabricated microelectronic devices. For very tiny amount of residual photoresist, neither the dark-field (Figure 6a) nor bright-field (Figure 6b) optical microscope can prove its existence. However, it can be easily discovered using the VCA technique (Figure 6c). Because photoresist is more hydrophobic than the silicon substrate, the areas with photoresist appear darker, while the areas without photoresist appear brighter. After annealing in air at 400 °C for 30 min, this substrate shows no dark contrast any more, indicating the photoresist is clearly removed (Figure 6d). This quick and effective VCA technique provides a very important method for the online quality assessment in semiconductor industry.

In summary, we have developed a technique to observe nanostructures by optical microscopy with the help of water vapor condensation. Essentially, we do not directly observe the nanostructures themselves but the condensation nuclei on them. The difference in the density and the type of the subnanometer condensation nuclei leads to different contrast under an optical microscope. In fact, the vapor molecule we used is not restricted to water. Any other vapor that meets the following conditions is acceptable: (i) the vapor should be easy to condense and easy to evaporate; (ii) the vapor should be more likely to condense either onto the nanostructure or onto the substrate, therefore to form a contrast between the nanostructure and the substrate. The limitations of the current VCA imaging technique include (i) the resolution is limited by the resolution of optical microscope; (ii) compared with some recently developed techniques,[19−21] it cannot provide information such as conductivity, bandgap, and chiral indices. Despite these limitations, this simple, low-cost, and efficient VCA approach is applicable to a variety of nanostructures, even to functional groups, and does not induce any impurities to the specimens, which will pave the way for widespread applications.

Methods. *VCA Optical Microscopy.* The optical imaging was carried out using an Olympus BX51M, which can work in both the bright-field mode and the dark-field mode. The simplest way to blow water vapor to the substrate is to puff by mouth. Actually, that was how we discovered this novel phenomenon. However, the water vapor blown by mouth inevitably contains some impurities. To guarantee the cleanness

dx.doi.org/10.1021/nl5016969 | *Nano Lett.* 2014, 14, 3527−3533

of CNTs as well as the substrate, we built a simple water-vapor-blowing apparatus by connecting a segment of thin glass tube with a rubber bulb. Inside the glass tube, we put some clean cloth soaked with deionized water. While outside the glass tube, some resistance wire was winded in order to heat the water inside the tube to a temperature slightly higher than room temperature. Thus, by squeezing the rubber bulb, clean and warm water vapor would flow out of the glass tube and condense into water droplets when it reaches the relatively cool substrate. To lengthen the lasting time of the image, we put some ice underneath the sample.

Other Characterization Techniques. To compare the optical microscope images with other characterization techniques, an SEM (FEI Sirion 200, operated at 1 kV) was used to characterize the ultralong CNTs on the substrate and the silicon substrate treated by oxygen plasma. An AFM (Nanoscope 5) was used in the tapping mode to measure the thickness of deposited amorphous carbon layer. An XPS (ESCALAB 250Xi) was used to detect the functional groups of the treated and untreated silicon substrates.

Synthesis of Ultralong CNTs. The ultralong CNTs were grown by a CVD method similar to that in our previous work.[16] As the "kite mechanism" shows,[17,18] the catalysts are suspended in air during the growth. Therefore, the substrate makes little difference to the growth. So different kinds of substrates might be chosen to load ultralong CNTs, such as naturally oxidized silicon wafers, silicon wafers with a thermal oxide layer of 500 nm, silicon wafers with a silicon nitride layer of 100 nm, or silicon wafers with a thermal oxide layer further deposited with Al or Ti. After the growth of CNTs, the samples were annealed at 80 °C in a low-pressure environment for 5 min to make the substrates more hydrophobic.

Transformation of Substrates to More Hydrophilic Ones. The hydrophilicity of substrates does not simply depend on the outermost layer of the substrate but can be modified by physical or chemical treatments afterward as well.[13−15] For example, silicon substrates with an outermost layer of Al or Ti can be turned to more hydrophilic by annealing in H_2 at 700 °C for 10 min.

Deposition of Amorphous Carbon and Fe. Amorphous carbon was deposited onto the silicon substrate using a homemade magnetron sputtering system. Fe was deposited onto the substrate by an e-beam evaporator.

Oxygen Plasma Treatment. Oxygen plasma treatment was realized in a reactive ion etching (RIE) system. The pressure of oxygen was 2 Pa. The output power is 30 W and the treatment lasted for 30 s.

■ ASSOCIATED CONTENT

Supporting Information

The videos of the VCA imaging process of as-grown ultralong CNTs and clean ultralong CNTs on the substrate. This material is available free of charge via the Internet at http://pubs.acs.org.

■ AUTHOR INFORMATION

Corresponding Authors

*E-mail: (Y.W.) WeiYang@tsinghua.edu.cn.
*E-mail: (K.J.) JiangKL@tsinghua.edu.cn.

Author Contributions

The manuscript was written through contributions of all authors. All authors have given approval to the final version of the manuscript.

J.W. and T.L. contributed equally to this work.

Notes

The authors declare no competing financial interest.

■ ACKNOWLEDGMENTS

This work was supported by the National Basic Research Program of China (2012CB932301) and NSFC (51102144, 11274190, 51102147, 90921012). We thank Professor Lin Feng for discussion and help on contact angle measurement.

■ ABBREVIATIONS

VCA, vapor-condensation-assisted; SEM, scanning electron microscope; TEM, transmission electron microscope; AFM, atomic force microscope; STM, scanning tunneling microscope; CNT, carbon nanotube; CVD, chemical vapor deposition; XPS, X-ray photoelectron spectrum; RIE, reactive ionic etching

■ REFERENCES

(1) Smith, K.; Oatley, C. W. *Br. J. Appl. Phys.* **1955**, *6* (11), 391−399.
(2) Knoll, M.; Ruska, E. *Z. Phys.* **1932**, *78* (5−6), 318−339.
(3) Binnig, G.; Quate, C. F.; Gerber, C. *Phys. Rev. Lett.* **1986**, *56* (9), 930−933.
(4) Binning, G.; Rohrer, H.; Gerber, C.; Weibel, E. *Phys. Rev. Lett.* **1982**, *49* (1), 57−61.
(5) Chang, N. K.; Hsu, J. H.; Su, C. C.; Chang, S. H. *Thin Solid Films* **2009**, *517* (6), 1917−1921.
(6) Huang, S. M.; Qian, Y.; Chen, J. Y.; Cai, Q. R.; Wan, L.; Wang, S.; Hu, W. B. *J. Am. Chem. Soc.* **2008**, *130* (36), 11860−11861.
(7) Chu, H. B.; Cui, R. L.; Wang, J. Y.; Yang, J. A.; Li, Y. *Carbon* **2011**, *49* (4), 1182−1188.
(8) Zhang, R. F.; Zhang, Y. Y.; Zhang, Q.; Xie, H. H.; Wang, H. D.; Nie, J. Q.; Wen, Q.; Wei, F. *Nat. Commun.* **2013**, *4*, 1727.
(9) Wilson, C. T. R. *Proc. R. Soc. London, Ser. A* **1911**, *85* (578), 285−288.
(10) Wilson, C. T. R. *Proc. R. Soc. London, Ser. A* **1912**, *87* (595), 277−292.
(11) Brintlinger, T.; Chen, Y. F.; Durkop, T.; Cobas, E.; Fuhrer, M. S.; Barry, J. D.; Melngailis, J. *Appl. Phys. Lett.* **2002**, *81* (13), 2454−2456.
(12) Zhang, R. Y.; Wei, Y.; Nagahara, L. A.; Amlani, I.; Tsui, R. K. *Nanotechnology* **2006**, *17* (1), 272−276.
(13) Kissinger, G.; Kissinger, W. *Phys. Status Solidi A* **1991**, *123* (1), 185−192.
(14) Amirfeiz, P.; Bengtsson, S.; Bergh, M.; Zanghellini, E.; Borjesson, L. *J. Electrochem. Soc.* **2000**, *147* (7), 2693−2698.
(15) Suni, T.; Henttinen, K.; Suni, I.; Makinen, J. *J. Electrochem. Soc.* **2002**, *149* (6), G348−G351.
(16) Wang, X. S.; Li, Q. Q.; Xie, J.; Jin, Z.; Wang, J. Y.; Li, Y.; Jiang, K. L.; Fan, S. S. *Nano Lett.* **2009**, *9* (9), 3137−3141.
(17) Huang, S. M.; Cai, X. Y.; Liu, J. *J. Am. Chem. Soc.* **2003**, *125* (19), 5636−5637.
(18) Huang, S. M.; Woodson, M.; Smalley, R.; Liu, J. *Nano Lett.* **2004**, *4* (6), 1025−1028.
(19) Li, J.; He, Y.; Han, Y.; Liu, K.; Wang, J.; Li, Q.; Fan, S.; Jiang, K. *Nano Lett.* **2012**, *12* (8), 4095−4101.
(20) He, Y. J.; Zhang, J.; Li, D. Q.; Wang, J. T.; Wu, Q.; Wei, Y.; Zhang, L. N.; Wang, J. P.; Liu, P.; Li, Q. Q.; Fan, S. S.; Jiang, K. L. *Nano Lett.* **2013**, *13* (11), 5556−5562.
(21) Liu, K. H.; Hong, X. P.; Zhou, Q.; Jin, C. H.; Li, J. H.; Zhou, W. W.; Liu, J.; Wang, E. G.; Zettl, A.; Wang, F. *Nat. Nanotechnol.* **2013**, *8* (12), 917−922.